



Published in final edited form as:

Med Phys. 2018 November ; 45(11): 5244–5250. doi:10.1002/mp.13170.

Technical Note: Feasibility of the *In vivo* Young's modulus visualization of pancreatic ductal adenocarcinoma during HIFU ablation Using Harmonic Motion Elastography (HME) in vivo

Alireza Nabavizadeh¹, Thomas Payen¹, Niloufar Saharkhiz¹, Matthew McGarry¹, Kenneth P Olive^{2,3}, and Elisa E Konofagou^{1,3}

¹Biomedical Engineering, Columbia University, USA

²Departments of Medicine and Pathology & Cell Biology, Herbert Irving Comprehensive Cancer Center, Columbia University Medical Center, USA

³Department of Radiology, Columbia University Medical Center, USA

Abstract

Purpose: Non-invasive quantitative assessment of coagulated tissue during HIFU (High Intensity Focused Ultrasound) ablation is one of the essential steps for tumor treatment, especially in such cases as the Pancreatic Ductal Adenocarcinoma (PDA) that has low probability of diagnosis at the early stages and high probability of forming solid carcinomas resistant to chemotherapy treatment at the late stages.

Methods: Harmonic motion elastography (HME) is a technique for the localized estimation of tumor stiffness. This harmonic motion imaging (HMI)-based technique is designed to map the tissue Young's modulus or stiffness noninvasively. A focused ultrasound (FUS) transducer generates an oscillating, acoustic radiation force in its focal region. The 2D shear wave speed, and consequently the Young's modulus maps, are generated by tracking the radio-frequency (RF) signals acquired at high frame rates. By prolonging the sonication for more than 50 s using the same methodology, the 2D Young's modulus maps are reconstructed while HIFU is applied and ablation is formed on PDA murine tumors.

Results: The feasibility of this technique in measuring the regional Young's modulus was first assessed in tissue-mimicking phantoms. The Contrast-to-noise ratio (CNR) was found to be higher than 25.2 dB for each 2D reconstructed Young's modulus map. The mean error in this validation study was found to be equal to less than 19 %. Then HME was applied on two transgenic mice with pancreatic ductal adenocarcinoma tumors. The Young's modulus median value of this tumor at the start of the HIFU application was equal to 2.1 kPa while after 45 s of sonication it was found to be approximately three times stiffer (6.7 kPa).

Conclusions: HME was described here in and showed its capability of measuring tissue stiffness noninvasively by measuring the shear wave speed propagation inside the tissue and reconstructing a 2D Young's modulus map. Although using the Harmonic Motion Imaging (HMI)

method to measure the Young's modulus is not new [14], applying the methodology in vivo and during HIFU, were performed here for the first time.

1. Introduction

Ultrasound-based elastography methods for mechanical evaluation of soft tissues can be categorized in two main groups based on their excitation methods: static and dynamic techniques. These methods have been applied on different tissues to assess their mechanical properties [1]. In addition, Magnetic Resonance Elastography (MRE) methods have also been reported on various organs like the brain, liver, heart, and muscle to evaluate their mechanical properties including, in clinical studies in patients [2–5].

Shear wave ultrasound elastography is a type of dynamic elastography, in which the mechanical properties of the tissues can be estimated by using radiation force to introduce shear waves and measuring the shear and Young's moduli by tracking the generated shear waves [6]. Based on some general assumptions that soft tissues are incompressible, isotropic, linearly elastic (i.e., ignoring shear wave dispersion), the Young's modulus, E , is related to shear wave propagation speed, C_s , as follows:

$$E = 3\rho C_s^2, \quad (1)$$

where ρ is the density assumed to be 1000 kg/m^3 for all soft tissues [6].

Different methods have been developed based on this type of excitation such as Shear Wave Elasticity Imaging (SWEI), [7, 8], Acoustic Radiation Force Imaging (ARFI), [9, 10], Supersonic Shear Imaging (SSI) [11], Shear wave Dispersion Ultrasound Vibrometry (SDUV) [12], and Comb-push Ultrasound Shear Elastography (CUSE) [13], in which the radiation force and its resulting shear wave is used to evaluate the viscoelastic tissue properties.

Harmonic Motion Imaging (HMI) is an ultrasound-based elastography technique that uses a focused ultrasound (FUS) transducer to generate an oscillatory radiation force at its focal point. The radiation force can be described by

$$F = \frac{2\alpha I}{c}, \quad (2)$$

where F is the radiation force generated (N), α is the tissue absorption coefficient (m^{-1}), I is the average acoustic intensity (W m^{-2}) and c is the sound speed (m s^{-1}).

Vappou et.al [14] proposed a quantitative method to measure the storage and loss modulus based on shear wave phase velocity estimation. Also, in more recent work by our group [15], the Young's modulus was estimated based on the radiation force and its resulting local axial strain. Moreover, in recent study by Wang *et al.* [16] strain elastography was used to assess the internal tumor pressure.

The aim of this study is to introduce a quantitative HMI-based method called Harmonic Motion Elastography (HME) to map the Young's modulus using the speed of the shear wave generated by the HMI radiation force. This Shear-wave-based method is capable of reconstructing a 2D Young's modulus map based on harmonic motion created by the FUS transducer during either imaging or ablation procedure. It should be noted that although applying HMI and measuring local displacement can assist in the relative local tissue stiffness, a quantitative modulus estimation technique like HME could render it more robust regarding surrounding boundary conditions.

In this paper, we first introduce the HME method and describe the method steps in more detail. Then, a phantom study was conducted for HME method validation. Finally, the HME method is applied to image the Young's modulus changes using an in vivo transgenic mouse model with PDA tumor and its local Young's modulus alteration during ablation is presented.

2. Materials and methods

2.A. Harmonic Motion Elastography Technique

The setup consists of an imaging transducer located confocally in the middle of the 93-element, FUS transducer ($f_c = 4.5$ MHz, and $D = 70$ mm, Sonic Concepts Inc., Bothell WA, USA). The imaging transducer was either a 64-element phased array imaging probe ($f_c = 2.5$ MHz, P4-2, ATL/Philips, Bothell, WA, USA) or a 104-element diagnostic transducer ($f_c = 7.8$ MHz, P12-5, ATL/Philips, Bothell, WA, USA). The former one was used in phantoms while the latter one in mice. The FUS transducer is driven by an AM sinusoidal signal. A dual-channel arbitrary waveform generator (AT33522A, Agilent Technologies Inc., Santa Clara, CA, USA) generates this AM signal through a 50dB power amplifier (325LA, E&I, Rochester, NY, USA).

The total acoustic power output of the FUS transducer was in the range of 6.4–8.6 W based on radiation-force balance measurements [17]. The oscillatory motion generated by the FUS transducer is estimated by the channel data acquired by the imaging transducer (Vantage, Verasonics, and Bothell, WA, USA). To reconstruct each RF data frame the acquired channel data matrix is multiplied by the reconstruction sparse matrix and its product matrix is multiplied by another sparse matrix for scan conversion [18].

The whole process is implemented in Graphical Processing Unit (GPU) [18].

During this process, the data are up sampled at either 80 MHz for a 64-element phased array or 125 MHz for a 104-element transducer [18]. The axial displacements at the focal point are estimated by applying 1-D normalized cross correlation on the reconstructed RF data [19]. To generate the 2D Young's modulus map, the same HMI displacement data of each point is used. Although it is possible to observe the shear wave propagation of the HMI displacement cineloop, a complex field of shear waves is generated due to constructive and destructive interaction of forward and reflected shear waves. To extract the shear wave from such a complex field, a directional filter is used to separate the leftward from the rightward shear waves. Because this spatio-temporal filter is capable of disassembling the generated

complex wave field into its components, traveling in various directions [20]. The filter was designed in frequency space with ability of choosing the portion of the wave with certain direction [21]. In addition, this filtering method helps in minimizing the standing wave. These advantages contributes considerably in reconstruction of shear modulus of the medium.

The final Young's modulus 2D map is the result of applying this filter on HMI displacement data and using the time-of-flight algorithm to measure, the time delay of the shear wave propagation by cross-correlating the filtered particle displacement profiles along the lateral direction. Then, two points separated by 8 and 6 ultrasound wavelengths, in the phantom and mouse study, respectively, at the same depth, are used to calculate the time that it takes the shear wave to travel between these two points. Then, based on the estimated time delay between these points at known distance, the shear wave speed is measured [13, 22]. The measured shear wave is assigned for the center pixel of the grid [22].

The 2D shear wave map is generated for each HMI measurement and the final 2D Young's modulus is reconstructed based on that.

2.B. Tissue mimicking phantom study

A customized CIRS phantom (Model 049 A) with a cylindrical lesion of 5 mm diameter was used. The Young's modulus for the background and inclusion part in the phantom with the stiffer inclusion was 5 ± 1 kPa, and 40 ± 8 kPa, respectively. In the second phantom with a softer inclusion, the Young's modulus of the inclusion was 10 ± 2 kPa and its background Young's modulus is the same as the stiffer phantom, 5 ± 1 kPa.

In this phantom study, the radiation force was applied for 0.6 s using an amplitude-modulated waveform with acoustic intensity of 1050 W/cm^2 and frequency of 25 Hz, resulting in excitation frequency of $f=50$ Hz [17, 23]. The imaging probe recorded plane waves at 1000 frames/second throughout the force application. We repeated the experiment five times by relocating the CIRS phantoms and changing the probe positions. The relative error based on

$$Error(\%) = \frac{E_F - E_H}{E_F} * 100, \quad (3)$$

where E_F is the Young's modulus of the CIRS phantom and E_H is the Young's modulus measured by HME method.

In addition, the contrast to noise ratio (CNR) was estimated based on [24]

$$CNR(dB) = 20 \log \frac{2(E_i - E_b)^2}{\sigma_i^2 + \sigma_b^2}, \quad (4)$$

where E_i and E_b are the mean Young's modulus of the inclusion and background, respectively; the σ_i and σ_b are the standard deviation of the Young's modulus of the inclusion and background.

2.E. *In vivo* ablation experiment on transgenic mice with PDA tumor

The Institutional Animal Care and Use Committee (IACUC) of Columbia University approved all animal studies presented herein. The developed pancreatic tumor in these mice models (K-rasLSL.G12D/+; p53R172H/+; PdxCre (KPC)) has been proved to be pathophysiologically similar to human pancreatic tumor [25]. Before starting the ablation, these KPC mice were abdominally depilated and laid supine on heat pad under isoflurane anesthesia and covered with ultrasound gel. First, an 18.5 MHz diagnostic probe (L22-14v, Verasonics, Bothell, WA, USA) was mounted on a 3D positioner and used to locate the pancreas and its surrounding organs due to its high-resolution B-mode image. In order to align the HMI images with high-resolution B-mode images, they were spatially registered with the high-resolution B-mode image by replacing this L22-14v transducer with the 104-element phased array ($f_c = 7.8$ MHz, P12-5, ATL/Philips, Bothell, WA, USA) without any change in the animal setting. This transducer was used for acquiring the frames while using HME. The FUS transducer was active for more than 60 seconds during the treatment at the same acoustic power.

3. RESULTS

3.A. Phantom study

In order to validate the HME methods, two modified CIRS phantoms (Model 049 A) with cylindrical lesion of 5 mm diameter were used. Figure 2 demonstrates the 2D Young's modulus reconstructed maps of these two phantoms using the HME method. The results are shown in Table 1. According to Table 1, the overall, largest, error for the inclusion and background part is under 19 % (Eq. 2).

In addition, the contrast to noise ratio (CNR) was higher than 25.4 dB (Eq. 3). In the second CIRS phantom, the relative error for both the inclusion and background was less than 10 % (Eq. 3)

3.C. *In vivo* tumor studies

Figure 3(a) shows the high resolution B-mode image of the pancreatic tumor, which is specified with white dashed oval and its surrounding organs. In this figure, the spleen and kidney are labeled with S and K, respectively. The ablation was performed on this tumor. At the end of the ablation the resulting 2D absolute peak-to-peak displacement map and its corresponding 2D Young's modulus map are shown in part (b) and (c) of this figure, respectively.

It should be noted the 2D maps shown in Figure 3 were reconstructed at the end of the HIFU application (after 57 s) in the first mouse study. However, in order to monitor the stiffness changes occurring while performing the HIFU ablation method the resulting 2D Young's

modulus map were reconstructed every nine seconds during HIFU ablation. The reconstructed 2D Young's modulus overlaid on the B-mode images is illustrated in figure 4.

Moreover, in figures 5 and 6, the temporal profile of the whole tumor specified with red dashed oval shapes is demonstrated based on the both absolute peak-to-peak displacement and Young's modulus estimation in the first and second *in vivo* mouse study respectively.

In both figures, the absolute peak-to-peak displacement and Young's modulus changes are in good agreement. The softer part shows higher displacement and lower Young's modulus while the stiffer areas have lower displacement and higher Young's modulus.

4. DISCUSSION

Ultrasound-based shear wave elastography methods in which the shear wave speed measurement is used for mechanical evaluation of soft tissues are becoming increasingly widespread due to their ease-of-use and ability to provide a quantitative 2D map of mechanical properties [26, 27]. Shear waves propagate faster in stiffer homogenous tissues comparing to softer ones [26, 27]. This difference in speed can be used to distinguish between normal and abnormal parts in tissue.

Generally, one of the common problems among all shear-wave-based elastography methods is the shear wave attenuation, which generates some artifacts in measuring shear wave speed [13]. Using harmonic radiation force at a low frequency, 25 Hz, to generate shear wave can address the attenuation problem [28].

The harmonic displacement generated during HMI and also HME application contributes significantly to elevate the signal-to-noise ratio (SNR) especially *in vivo* and deep-seated organs while attenuation problem poses a formidable challenge for other ultrasonic shear wave methods [8–13,27]. Using the same FUS transducer to apply a harmonic and continuous radiation force will result in a continuous harmonic displacement. This continuity and harmonic nature of applied push contributes significantly to increase the signal-to-noise ratio (SNR) especially *in vivo* and deep-seated organs while attenuation problems pose a formidable challenge for other ultrasonic shear wave methods [8–13,27].

Furthermore, the use of a FUS transducer instead of an imaging one for radiation force application or FUS-push has a substantial impact to overcome those limitations [28] also, when it comes to lateral propagation, the estimation errors increase by propagating away from the perturbation region due to the lack of sufficient displacement [28]. In addition, in HME, there is inherent registration between perturbation and the detection parts and no concern about damaging the probe because of high power application.

Due to the geometry of the FUS transducer, the resulting focal point is more focused. This characteristic helps to generate waves in all directions symmetrically. Moreover, the cylindrical symmetry of the shear wave front can partially assist in lowering the attenuation effect and increasing the accuracy of the shear modulus and Young's modulus estimation of the medium [29, 30]. Also, it should be noted that the measured 2D Young's modulus map in the HME method is completely independent of the magnitude of applied radiation force

or consequently the resulted absolute peak-to-peak displacement measurement. In this study, we showed that the HME technique could estimate the Young's modulus of the tissue under ablation by measuring the speed of resulting shear wave. In other words, instead of having a transient push, which is very common among the aforementioned ultrasonic shear wave methods because of using the imaging transducer for that purpose, in HME method, a continuous push is applied separately by a FUS transducer while the RF signal is recorded by imaging transducer. This combination helps to overcome those limitations.

HIFU cannot only be used to generate ablation but as a source to generate the shear wave and subsequently 2D Young's modulus map.

The displacement and Young's modulus monitoring of *in vivo* tumor ablation confirms that a progressive softening- then- stiffening indicated by displacement increase-then-decrease and Young's modulus decrease-then-increase occurred figs.(5 and 6). This trend happens not only for tumor part as it is clear in figure 4, the similar changes happened to background part too.

The results also show the softened area around the lesion boundary (Fig. 3) [23, 31, 32]. In addition, it should be noted that the speed of sound does not have any effects in displacement measurement in HMI and HME method [33, 34]. However, some artifacts are apparent in figures 3 and 4 but it is interesting that using two different imaging methods: absolute peak-to-peak displacement (Fig. 3(b)) and HME, (Fig. 3(c)) depict similar results.

Furthermore, it is worth to mention here that in Fig. 3 (b), the peak-to-peak displacement value was not measured for background part because there was no raster scanning involved and the push was applied only in a single location at the center of the tumor. This is complementary information provided by HME as it is shown in Fig. 3 (c); only one push is enough to measure the stiffness of the medium while in conventional HMI method, raster scanning is necessary for stiffness evaluation of the medium.

Despite all the advantages that have been mentioned so far, in this study, we did not use any thermal assessment of the tissue during HIFU, because the goal was first to illustrate the feasibility of the HME method in reconstructing the 2D map of Young's modulus during the HIFU ablation.

Figure 4 demonstrates the reconstructed 2D maps at every 9 seconds at the onset of HIFU ablation process. Thus, ongoing work mostly focuses on the thermal ablation monitoring using the Young's modulus information during HIFU procedure.

The 2D Young's modulus map resulting from the HME method looks reliable. However, there are some factors involved in generating artifacts, which were apparent in Figs 3 and 4. Cavitation is a potential candidate. Because the generated bubbles could elevates the local pressure and result in a higher local [stiffness](#).in addition, as figure 3 shows the peak-to-peak displacement 2D map of tumor in which standing wave has no influence on its result shows the same trend as what has been illustrated in 2D Young's modulus map. Stiffer areas have higher Young's modulus and lower displacement while the softer one has lower Young's

modulus and higher displacement. It could be concluded that standing wave has a lower effect in creation of the artefacts in HME 2D maps.

5. Conclusion

An ultrasonic shear-wave-based technique using HMI was proposed. It was demonstrated that this radiation force technique was capable of reconstructing the 2D Young's modulus of the tissue, during and after ablation in vivo. Shear wave imaging for stiffness estimation is wide spread [1]. However, HME method is distinct from other shear wave methodology in the fact that it uses oscillatory force that can separate motion from breathing and body movement [30] as well as engage viscosity estimation [15].

Future studies will focus on measuring the Young's modulus in real time and using the Young's modulus for thermal and temperature assessment in in-vivo patient study.

Acknowledgements

The authors acknowledge Stephen A Sastra, and C F Palermo, at the Herbert Irving Comprehensive Cancer Center, Columbia University, for their assistance in the mouse study.

References

1. Li G-Y and Cao Y. Mechanics of ultrasound elastography in Proc. R. Soc. A 2017: The Royal Society.
2. M uthupillai R, Lomas DJ, Rossman PJ, Greenleaf JF, Manduca A, Ehman RL, 1995 Magnetic resonance elastography by direct visualization of propagating acoustic strain waves. *Science* 269, 1854–1857. [PubMed: 7569924]
3. Serai SD, et al., Repeatability of MR Elastography of Liver: A Meta-Analysis. *Radiology*, 2017: p. 161398.
4. Arani A, et al., Cardiac MR elastography for quantitative assessment of elevated myocardial stiffness in cardiac amyloidosis. *Journal of Magnetic Resonance Imaging*, 2017.
5. Chakouch MK, et al., Viscoelastic shear properties of in vivo thigh muscles measured by MR elastography. *Journal of Magnetic Resonance Imaging*, 2016 43(6): p. 1423–1433.. [PubMed: 26605873]
6. Skovorda A, et al., Quantitative analysis of mechanical characteristics of pathologically altered soft biological tissues. *Biofizika*, 1995 40(6): p. 1335–1340. [PubMed: 8590726]
7. Sarvazyan AP, Rudenko OV, Swanson SD, Fowlkes JB, and Emelianov SY, "Shear wave elasticity imaging: A new ultrasonic technology of medical diagnostics," *Ultrasound Med. Biol.*, vol. 24, pp. 1419–1435, Dec. 1998. [PubMed: 10385964]
8. Yoon H, Aglyamov SR, and Emelianov SY, Dual-phase transmit focusing for multi-angle compound shear-wave elasticity imaging. *IEEE transactions on ultrasonics, ferroelectrics, and frequency control*, 2017.
9. Nightingale K, McAleavey S, and Trahey G, Shear-wave generation using acoustic radiation force: in vivo and ex vivo results. *Ultrasound in medicine & biology*, 2003 29(12): p. 1715–1723. [PubMed: 14698339]
10. Goertz RS et al. Acoustic radiation force impulse shear wave elastography (ARFI) of acute and chronic pancreatitis and pancreatic tumor. *European journal of radiology* 85, 2211–2216 (2016). [PubMed: 27842669]
11. Bercoff J, Tanter M, and Fink M, Supersonic shear imaging: a new technique for soft tissue elasticity mapping. *IEEE transactions on ultrasonics, ferroelectrics, and frequency control*, 2004 51(4): p. 396–409.

12. Chen S, et al., Shearwave dispersion ultrasound vibrometry (SDUV) for measuring tissue elasticity and viscosity. *IEEE transactions on ultrasonics, ferroelectrics, and frequency control*, 2009 56(1): p. 55–62.
13. Song P, et al., Comb-push ultrasound shear elastography (CUSE): a novel method for two-dimensional shear elasticity imaging of soft tissues. *IEEE transactions on medical imaging*, 2012 31(9): p. 1821–1832. [PubMed: 22736690]
14. Vappou J, Maleke C & Konofagou EE Quantitative viscoelastic parameters measured by harmonic motion imaging. *Physics in medicine and biology* 54, 3579 (2009). [PubMed: 19454785]
15. Vappou J et al. Non-contact, ultrasound-based indentation method for measuring elastic properties of biological tissues using Harmonic Motion Imaging (HMI). *Physics in medicine and biology* 60, 2853 (2015). [PubMed: 25776065]
16. Wang H et al. Elastographic Assessment of Xenograft Pancreatic Tumors. *Ultrasound in medicine & biology* 43, 2891–2903 (2017). [PubMed: 28964615]
17. Payen T, et al., Elasticity mapping of murine abdominal organs in vivo using harmonic motion imaging (HMI). *Physics in medicine and biology*, 2016 61(15): p. 5741. [PubMed: 27401609]
18. Hou GY et al. Sparse matrix beamforming and image reconstruction for 2-D HIFU monitoring using harmonic motion imaging for focused ultrasound (HMIFU) with in vitro validation. *IEEE transactions on medical imaging* 33, 2107–2117 (2014). [PubMed: 24960528]
19. Luo J & Konofagou EE A fast normalized cross-correlation calculation method for motion estimation. *IEEE transactions on ultrasonics, ferroelectrics, and frequency control* 57, 1347–1357 (2010).
20. Manduca A, Lake DS, Kruse SA & Ehman RL Spatio-temporal directional filtering for improved inversion of MR elastography images. *Medical image analysis* 7, 465–473 (2003). [PubMed: 14561551]
21. Deffieux T, Gennisson J. I., Bercoff J & Tanter M On the effects of reflected waves in transient shear wave elastography. *IEEE transactions on ultrasonics, ferroelectrics, and frequency control* 58, 2032–2035 (2011).
22. Song P, et al., Fast shear compounding using robust 2-D shear wave speed calculation and multi-directional filtering. *Ultrasound in medicine & biology*, 2014 40(6): p. 1343–1355. [PubMed: 24613636]
23. Han Y, et al., Fast lesion mapping during HIFU treatment using harmonic motion imaging guided focused ultrasound (HMIGFUS) in vitro and in vivo. *Physics in medicine and biology*, 2017 62(8): p. 3111. [PubMed: 28323638]
24. Varghese T, Ophir J, Konofagou E, Kallel F & Righetti R Tradeoffs in elastographic imaging. *Ultrasonic imaging* 23, 216–248 (2001). [PubMed: 12051276]
25. Olive KP et al. 2009 Inhibition of Hedgehog signaling enhances delivery of chemotherapy in a mouse model of pancreatic cancer *Science* 324 1457–61. [PubMed: 19460966]
26. Gao L, Parker KJ, Lerner RM, Levinson SF. 1996 Imaging of the elastic properties of tissue—a review. *Ultrasound Med. Biol* 22, 959–977. (doi:10.1016/S0301-5629(96)00120-2) [PubMed: 9004420]
27. Sarvazyan A, Hall TJ, Urban MW, Fatemi M, Aglyamov SR, Garra BS. 2011 An overview of elastography - an emerging branch of medical imaging. *Curr. Med. Imaging Rev.* 7, 255–282. (doi: 10.2174/157340511798038684) [PubMed: 22308105]
28. Iwasaki R, et al., Monitoring of high-intensity focused ultrasound treatment by shear wave elastography induced by two-dimensional-array therapeutic transducer. *Japanese Journal of Applied Physics*, 2016 55(7S1): p. 07KF05.
29. Nabavizadeh A, Song P, Chen S, Greenleaf JF & Urban MW Multi-source and multi-directional shear wave generation with intersecting steered ultrasound push beams. *IEEE transactions on ultrasonics, ferroelectrics, and frequency control* 62, 647–662 (2015).
30. Nabavizadeh A, Greenleaf JF, Fatemi M & Urban MW Optimized shear wave generation using hybrid beamforming methods. *Ultrasound in medicine & biology* 40, 188–199 (2014). [PubMed: 24139918]
31. Chen H et al. Harmonic motion imaging for abdominal tumor detection and high-intensity focused ultrasound ablation monitoring: an in vivo feasibility study in a transgenic mouse model of

- pancreatic cancer. *IEEE transactions on ultrasonics, ferroelectrics, and frequency control* 62, 1662–1673 (2015).
32. Hou GY, Marquet F, Wang S, Apostolakis I-Z & Konofagou EE High-intensity focused ultrasound monitoring using harmonic motion imaging for focused ultrasound (HMIFU) under boiling or slow denaturation conditions. *IEEE transactions on ultrasonics, ferroelectrics, and frequency control* 62, 1308–1319 (2015).
 33. Shahmirzadi D, Hou GY, Chen J, and Konofagou EE, “Exvivo characterization of canine liver tissue viscoelasticity after highintensity focused ultrasound ablation,” *Ultrasound Med. Biol.*, vol. 40, no. 2, pp. 341–350, Feb. 2014. [PubMed: 24315395]
 34. Maleke C and Konofagou EE 2008 Harmonic motion imaging for focused ultrasound (HMIFU): a fully integrated technique for sonication and monitoring of thermal ablation in tissues *Phys. Med. Biol* 53 1773–93. [PubMed: 18367802]

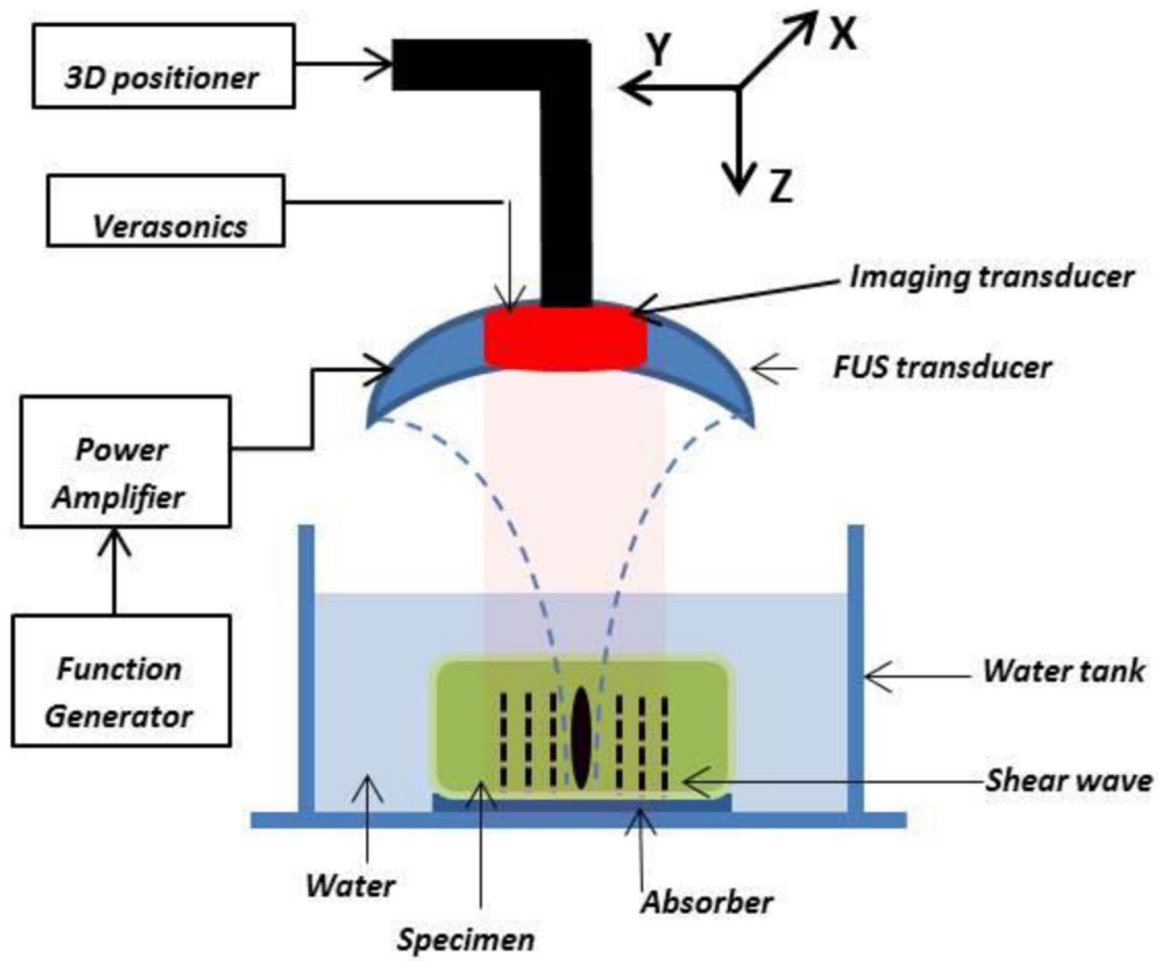


Figure 1.
Harmonic Motion Elastography (HME) setup

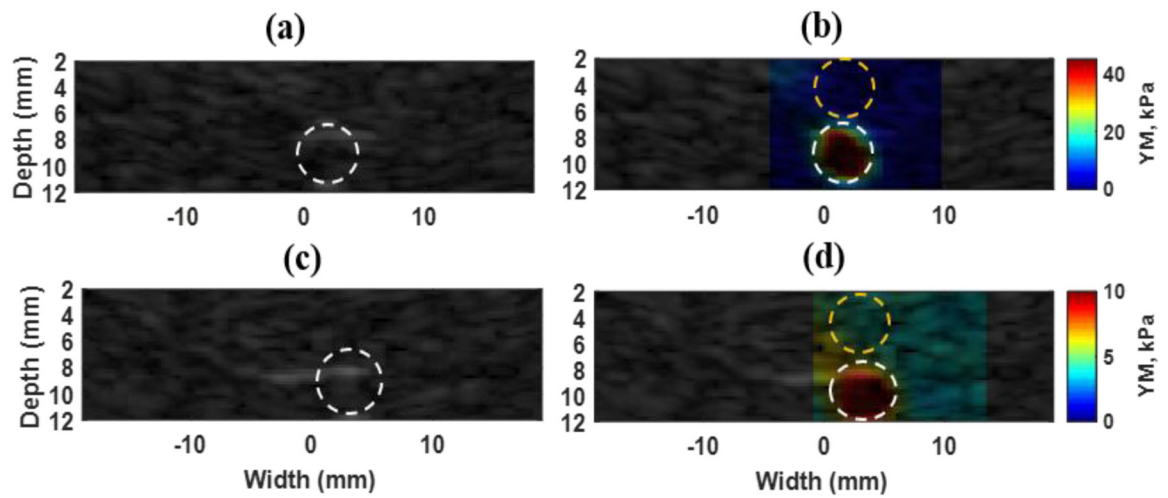


Figure 2.

(a) B-mode image of phantom with stiff inclusion, (b) Overlaid image of reconstructed 2D Young's modulus map on original B-mode in Phantom with a stiff inclusion. The estimated E , for background part specified with dashed yellow circle is 4.8 ± 0.9 kPa. the dashed white circle shows the lesion part and $E = 41.5 \pm 9.8$ kPa. (c) B-mode image of phantom with soft inclusion. (d) Overlaid image of reconstructed 2D Young's modulus map on original B-mode in phantom with a stiff inclusion. The estimated E , for background part specified with dashed yellow circle is 4.3 ± 0.3 kPa. The dashed white circle shows the lesion part and $E = 10.1 \pm 1$ kPa.

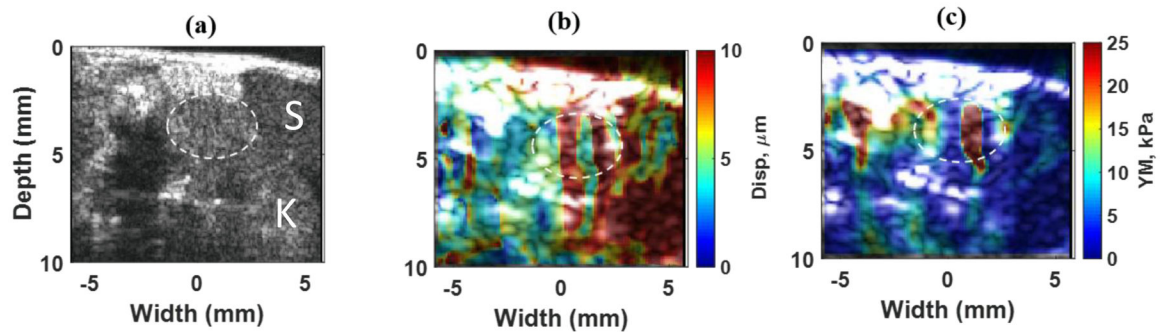


Figure 3.

(a) High resolution B-mode image of PDA tumor and surrounding organs using L22–14V probe. The tumor is specified with a dashed white oval shape. The spleen is as S and kidney as K. (b) 2D absolute peak-to-peak displacement map of the pancreatic tumor at the end of HIFU ablation ($t=57$ s) with the median value of $6.2 \mu\text{m}$. (c) 2D Young's modulus map at the end of HIFU ablation ($t=57$ s) with median value of 6.2 kPa for tumor part and 4.4 kPa for surrounded part.

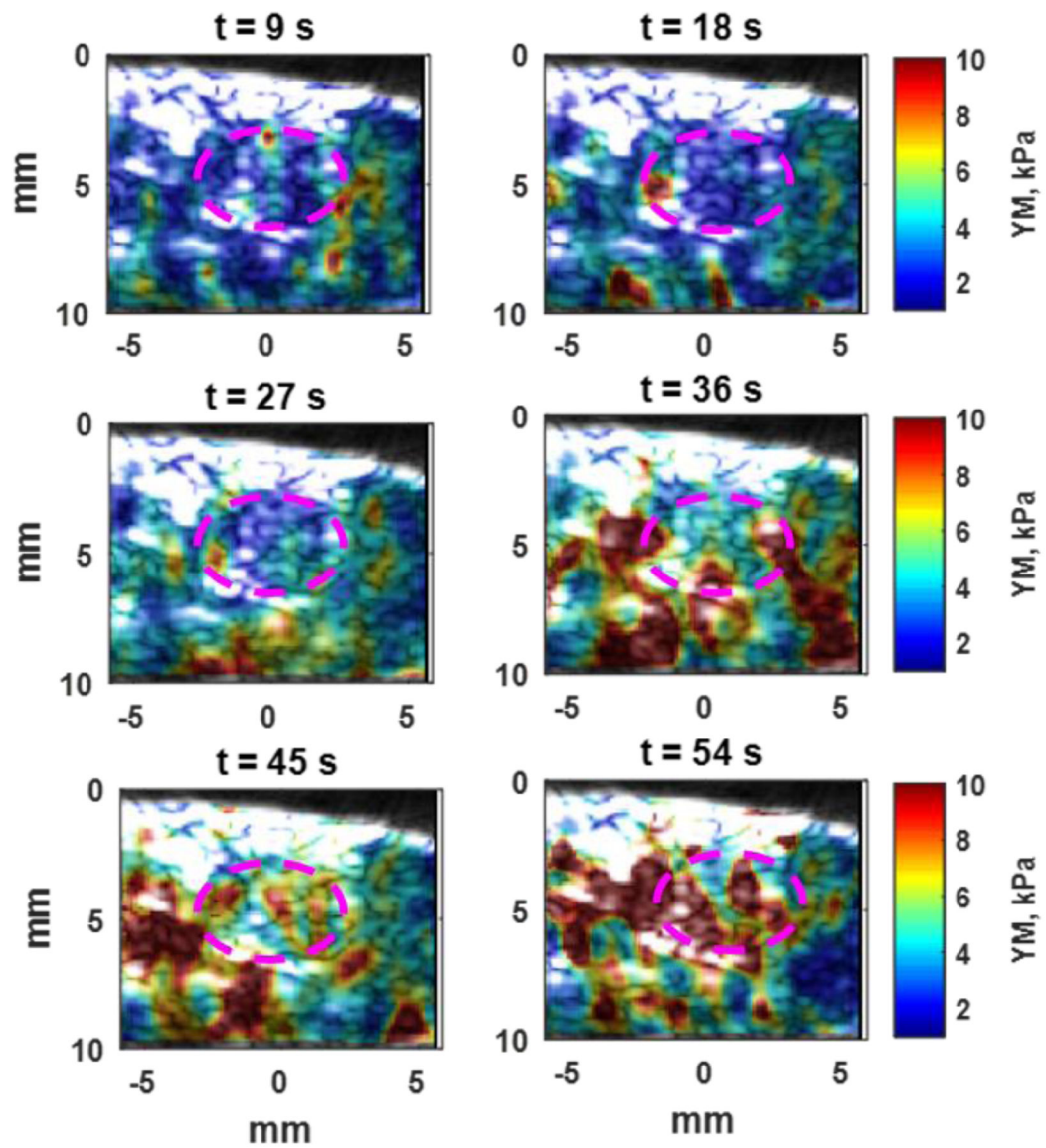


Figure 4. Overlay of 2D Young's modulus map of pancreatic tumor on low-resolution B-mode images as it has been in figure 3(a) with Purple dashed oval. After 9 seconds of HIFU ablation, the median Young's modulus is 1.9 kPa and after 54 seconds, increases to 6.7 kPa.

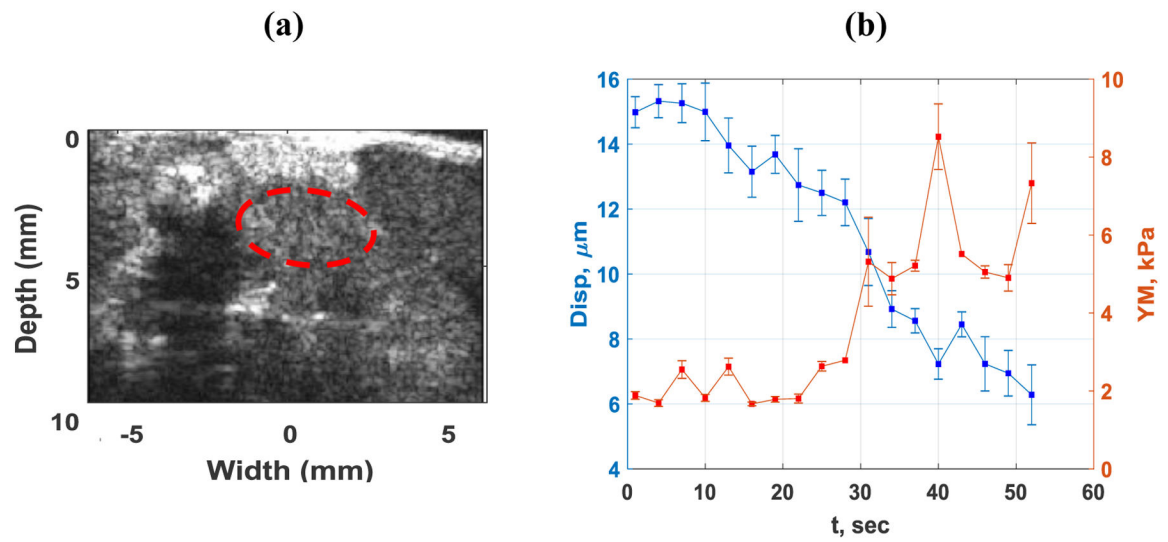


Figure 5.

(a) High resolution B mode image of PDA Tumor and surrounding organs of the first in vivo mouse study using L 22-14 V probe. The tumor is specified with a dashed red oval shape, (b) The absolute peak-to-peak displacement and Young's modulus temporal profiles of tumor, red dashed oval, in part (a) of this figure during HIFU application for 54 seconds.

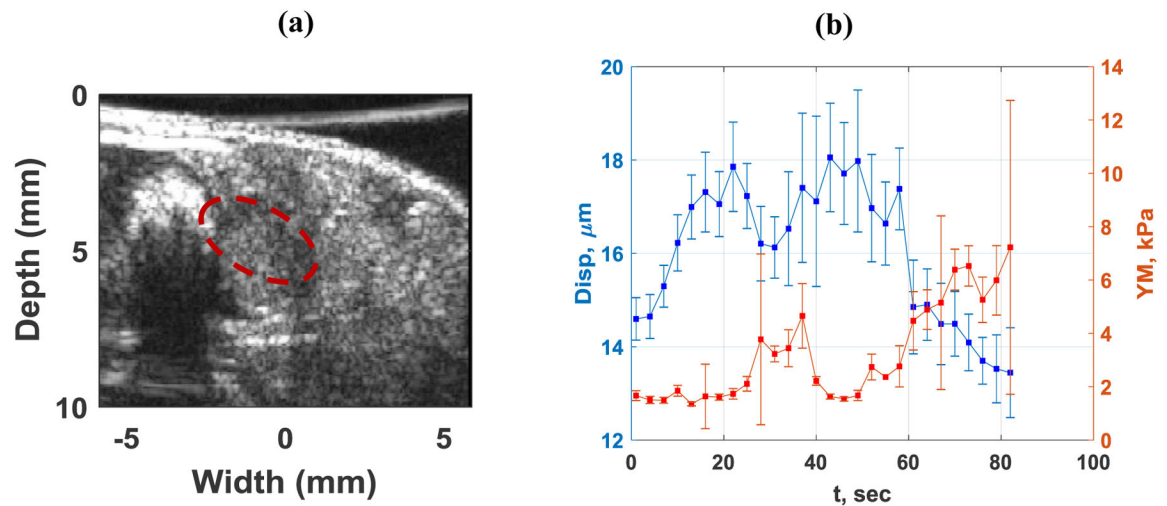


Figure 6.

(a) High resolution B-mode image of PDA tumor and surrounded organs of the second *in vivo* mouse study using L22-14V probe. The tumor is specified with a dashed red oval shape. (b) The absolute peak-to-peak displacement and Young's modulus temporal profiles of tumor, red dashed oval, in part (a) of this figure during HIFU application for 84 seconds.

Table. 1

Young's modulus, YM, values and contrast to noise ratio in CIRS phantom with stiffer inclusion

Trial	Inclusion (E_i)	Background (E_b)	Error, inclusion (%)	Error, Background (%)	CNR (dB)
1	41.5 ± 9.3	4.8 ± 0.9	4	4	31.8
2	44.0 ± 10.8	4.7 ± 0.8	10	6	30.3
3	32.5 ± 6.5	4.7 ± 0.9	19	6	33.6
4	36.8 ± 10.6	4.7 ± 0.7	8	6	27.5
5	36.6 ± 11.9	4.3 ± 0.3	8	14	25.4
AV	38.3 ± 9.8	4.6 ± 0.7	10	8	29.5

Author Manuscript

Author Manuscript

Author Manuscript

Author Manuscript